frontiers in Earth Science

ORIGINAL RESEARCH
published: 29 April 2021
doi: 10.3389/feart.2021.582062

Potential Production of Carbon Gases and Their Responses to Paleoclimate Conditions: An Example From Xiaolongtan Basin, Southeast Tibetan Plateau

Gen Wang[1,2], Yongli Wang[3,4], Zhifu Wei[1,2]*, Zepeng Sun[5], Wei He[1,6] and Xueyun Ma[1,6]*

[1] Northwest Institute of Eco-Environment and Resources, Chinese Academy of Sciences, Lanzhou, China, [2] Key Laboratory of Petroleum Resources, Gansu Province, Lanzhou, China, [3] Key Laboratory of Cenozoic Geology and Geophysics, Chinese Academy of Sciences, Beijing, China, [4] CAS Center for Excellence in Life and Paleoenvironment, Beijing, China, [5] College of Resources and Environment, Shanxi Agricultural University, Jinzhong, China, [6] College of Earth and Planetary Sciences, University of Chinese Academy of Sciences, Beijing, China

OPEN ACCESS

Edited by:
Francesco Italiano,
National Institute of Geophysics and Volcanology, Italy

Reviewed by:
Jens Kallmeyer,
Helmholtz Centre Potsdam, Germany
Weiguo Liu,
Chinese Academy of Sciences, China
Xianyu Huang,
China University of Geosciences, China
Zhang Chengjun,
Lanzhou University, China

***Correspondence:**
Yongli Wang
ylwang@mail.iggcas.ac.cn
Zhifu Wei
weizf@lzb.ac.cn

Specialty section:
This article was submitted to Biogeoscience, a section of the journal Frontiers in Earth Science

Received: 10 July 2020
Accepted: 08 April 2021
Published: 29 April 2021

Citation:
Wang G, Wang Y, Wei Z, Sun Z, He W and Ma X (2021) Potential Production of Carbon Gases and Their Responses to Paleoclimate Conditions: An Example From Xiaolongtan Basin, Southeast Tibetan Plateau. Front. Earth Sci. 9:582062. doi: 10.3389/feart.2021.582062

Uplift of the Tibetan Plateau plays a significant and lasting role in the variations of climate conditions and global carbon cycle. However, our knowledge is limited due to the lack of long-sequence records revealing rates of CO_2 and CH_4 production, hampering our understanding of the relationship between paleoclimatic conditions, carbon cycling and greenhouse gas flux. Here, we present a combination of paleoclimate records and low-temperature thermal simulation results from sediments of the Xiaolongtan Basin at the southeastern margin of the Qinghai-Tibetan Plateau, spanning the late Miocene (14.1 ∼ 11.6 Ma). The *n*-alkane-derived proxies suggested that the sources of organic matter were obviously different: a mixed source including lower organisms and terrestrial higher plants for the Dongshengqiao Formation from 14.1 to 12.6 Ma, and a predominant contribution from terrestrial higher plants for Xiaolongtan Formation between 12.6 and 11.6 Ma. The paleoclimate was generally warm and humid as reflected by the lipid biomarkers, consistent with previous studies. In addition, the carbon gases (including CO_2 and hydrocarbon gases) generated by the low-temperature thermal simulation experiments indicated a production rate of CO_2 and CH_4 were as high as 88,000 ml/kg rock and 4,000 ml/kg rock, respectively, implying there were certain amounts of carbon gases generated and released into the atmosphere during their shallow burial stage. Besides, the calculated production rate of carbon gases and the estimated burial flux of organic carbon varied in response to the variations of paleoclimate conditions. Based on these observations, we propose that the climate conditions predominantly controlled the formation and accumulation of organic matter, which consequently affected the production of carbon gases and burial flux of organic carbon. The results presented here may provide a significant insight into the carbon cycle in the southeast of the Tibetan Plateau.

Keywords: lipid biomarker, low-temperature thermal simulation, carbon cycle, burial rates of organic carbon, late Miocene

INTRODUCTION

In recent years, increasing attention was paid to global warming and greenhouse effects. The carbon cycle in relevant terrestrial ecosystem, especially the organic carbon inventory, has been becoming a focus and hotspot in the field of global climate research (Heimann and Reichstein, 2008; Fang et al., 2018). The production rates of CO_2 and CH_4 released from sediments caused by thermal maturation during their shallow burial stage are critical to improve our understanding about carbon cycling and greenhouse gas flux in terrestrial ecosystems (Wilson et al., 2019). Organic carbon storage can be significantly influenced by anthropogenic activities and/or climate variations, such as air temperatures, atmospheric CO_2 concentrations, precipitation patterns (Smoak et al., 2013; Ruiz-Fernández et al., 2018). Knowledge about how the organic carbon inventory responds to the shifts of climate conditions will definitely enhance our understanding of its variations under the background of global warming and increased human activities. Related studies mainly focused on marshes (Ruiz-Fernández et al., 2018), lake sediments (Xu et al., 2013; Yu et al., 2015; Zhang et al., 2018), coastal wetlands (Choi and Wang, 2004), marine sediments (Shao et al., 2016; Wang K. et al., 2019) reaching back only a few hundred years, with only a few records discussing the relationship over long time scales (Owens et al., 2018; Gao et al., 2019).

The Qinghai-Tibetan Plateau is a globally important terrestrial ecosystem, owing to its special location and continuous uplift during the Cenozoic, it exerts significant influence on the regional and even global climate. Located in the southeastern margin of the Tibetan Plateau, the Xiaolongtan Basin accumulated continuous strata of Cenozoic sediments (Wang et al., 1998), which can provide important information about the evolution of Indian monsoon and southeastward extension of the Tibetan Plateau (Tapponnier et al., 2001; Huang et al., 2016). However, studies about the variations of paleoclimate conditions and organic carbon inventory and their interactions were limited, resulted in patchy understanding of the environmental and uplift history as well as the organic carbon cycle in the southeastern margin of the Tibetan Plateau. Li S.H. et al. (2015) and Zhang et al. (2019) established the chronology for the Xiaolongtan Basin sequence, but the paleoclimate history had not been well documented. As a consequence, in the present study, we analyzed the lipid biomarkers, total organic carbon concentrations, and carried out low temperature thermal simulation experiments of the sediments from Xiaolongtan Basin, in order to gain insights into the evolution of paleoclimate conditions, and its influences on carbon gases (including CO_2 and CH_4) emissions and organic carbon burial rates in the southeastern Tibetan Plateau.

GEOLOGICAL SETTINGS

The Xiaolongtan Basin, located in the Honghe Hani and Yi Autonomous Prefecture, southeastern part of the Yunnan Province (**Figure 1**), is a typical pull-apart basin controlled by the Qujing fault to the east and the Xianshuihe–Xiaojiang fault to the west (Li S.H. et al., 2015), and has accumulated a thick sequence of sediments deposited in swamp-fluviolacustrine environment. The oldest Chinese hominoid fossils have been found in this sequence (Woo, 1987; Ji et al., 2013; Li S.H. et al., 2015). The average elevations of Xiaolongtan Basin and its surrounding mountains are about 1,000–1,150 m a.s.l. and 1,300–1,800 m a.s.l., respectively. At present, the Xiaolongtan Basin is characterized by a subtropical monsoon climate. The mean annual precipitation is about 770 mm, with an amount of 460 mm falling during the summer season. The mean annual temperature is about 20.1°C, with mean monthly temperatures of 24.5°C in July and 13.5°C in January (**Figure 1C**). The vegetation distributed around the basin is mainly composed of subtropical broad-leaved evergreen forest.

The Cenozoic stratigraphy of Xiaolongtan Basin can be divided into four formations according to its lithofacies and paleontology, including Dongshengqiao Formation, Xiaolongtan Formation, Buzhaoba Formation and Hetou Formation, from the bottom to the top (Dong, 2001). The lithology of Dongshengqiao Formation is light-gray clay in its middle-upper parts, above mudstone, sandstone and conglomerate. The Xiaolongtan Formation comprises black lignite and the Buzhaoba Formation is characterized by gray–white marl (Zhang et al., 2019). And the Hetou Formation is attributed to the Quaternary sediments, owing to the observation of fossil mammals in its sediments (Dong, 2001). The hominoid fauna in the Xiaolongtan Formation have been determined spanning the middle-late Miocene (Dong, 2001).

CHRONOLOGY

Li S.H. et al. (2015) reported a magnetostratigraphic study on the Xiaolongtan Formation in the Xiaolongtan Basin, and suggested the Xiaolongtan Formation sedimentary sequence spanned from Chron C5Ar.1r to Chron C5n.2n, ranging from 12.7 to ∼10 Ma. Recently, in combination with previous work, Zhang et al. (2019) carried out high-resolution magnetostratigraphy to the entire late Neogene fluvio-lacustrine sedimentary sequence in order to acquire the whole dates for the start and finish of sedimentation in the Xiaolongtan Basin. Their results revealed 11 reversed and 11 normal zones, covering Chron 5n.2n to Chron 5ACr, indicating that the whole stratigraphic sequence in the Xiaolongtan Basin ranges from ∼14.1 to ∼10.0 Ma. Specifically, the Dongshengqiao Formation was deposited between 14.1 and 12.6 Ma, and the Xiaolongtan Formation was accumulated from 12.6 to 11.6 Ma.

SAMPLING AND METHODS

Sampling

In the present study, we collected outcrop samples from the same sections described by Zhang et al. (2019), including sections Xiaolongtan-I (XLT-I) and Xiaolongtan-II (XLT-II). The XLT-I section, identified as Dongshengqiao Formation, is located in the Buzhaoba open-cast coal mine in the southern Xiaolongtan Basin, and accumulated strata of 198 m. The overall lithology

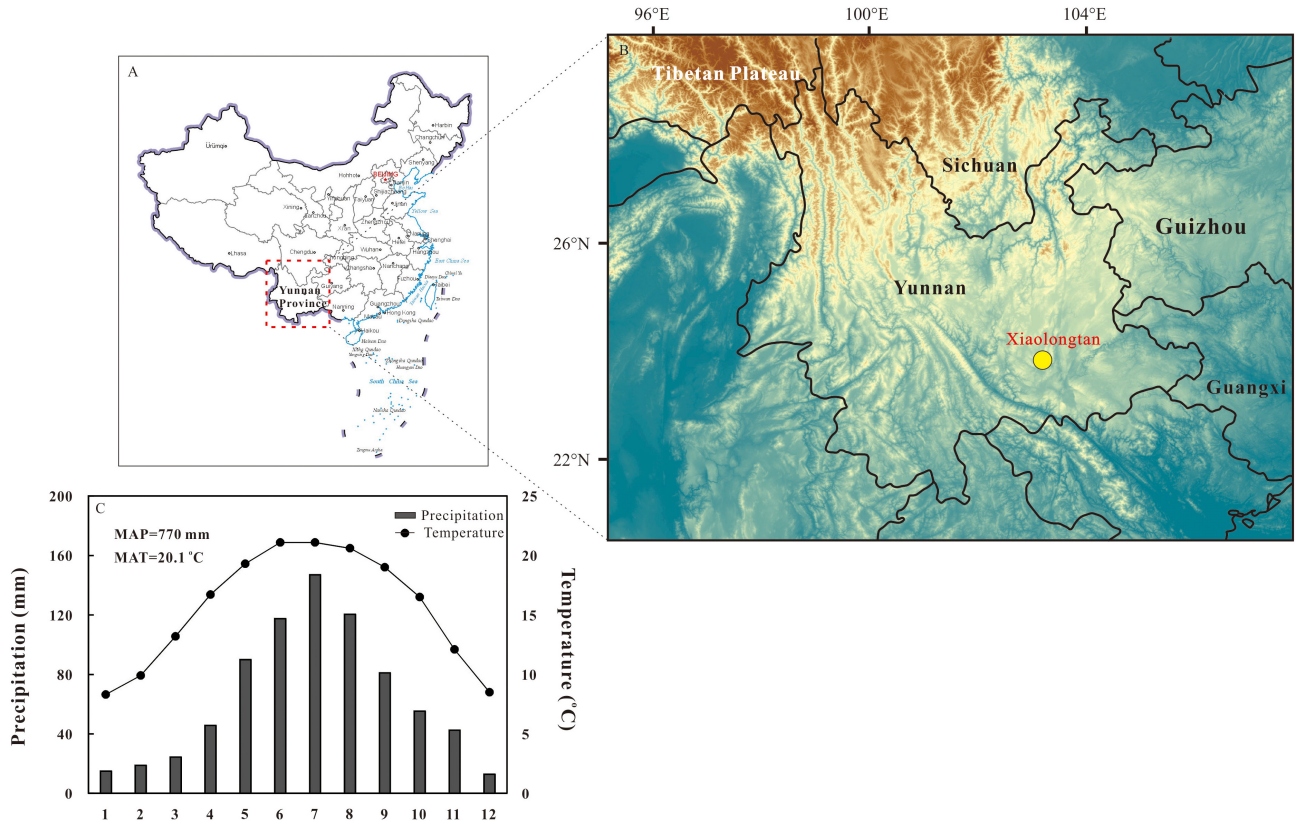

FIGURE 1 | (A) Location of Yunnan Province; **(B)** location of Xiaolongtan Basin in the Yunnan region at the southeast margin of the Tibetan Plateau; **(C)** mean monthly temperature and precipitation from Kaiyuan meteorological station from 1981 to 2010.

of this section mainly consists of brownish yellow and gray–white fine clay and sandstone, containing several thin layers of black coal. The XLT-II section, identified as Xiaolongtan Formation, is 161 m in thickness and exposed in the northern Xiaolongtan Basin. It is characterized by black lignite interbedded with several layers of mudstones. For further information please refer to Zhang et al. (2019).

MATERIALS AND METHODS

Total Organic Carbon (TOC) and Vitrinite Reflectance (Ro%)

An aliquot of each sample was acidified with HCl to remove carbonates before analysis. Then, samples were washed with deionized water until a neutral pH value was reached. Next, samples were dried in an oven at 90°C. Afterward, the treated samples were combusted using a CS-I analyzer (Eltra, Germany) in the Northwest Institute of Eco-Environment and Resources, Chinese Academy of Sciences. Before and during the analysis, standard samples (Carbon and Sulfur in Steel, produced by LECO CORPORATION, Carbon percent 0.881 ± 0.008; Sulfur percent 0.0155 ± 0.009) were applied to calibrate and monitor the accuracy of the CS-I analyzer. Precision was better than 0.03%.

The vitrinite reflectance measurements were conducted on a Leica DM2500P microscope equipped with MPM600 microphotometer following the standard SY/T 5124-2012. Appropriate reflectance standards in including cubic zirconia (3.13% Ro), N-LASF46A glass (1.31% Ro) and Yttrium-aluminum-garnet (0.91% Ro) were used for calibration.

Lipid Biomarkers

In order to avoid contamination during the organic matter extraction, all glassware was washed sequentially with detergent, chromic acid, tap water, distilled water and finally annealed at 450°C for 12 h in the muffle furnace. After air-drying and grinding the samples to about 150 μm, about 20 g were extracted continuously for 72 h with chloroform in a Soxhlet extractor. The solvent was purified by distillation. Afterward, the extracted organic matter was condensed and weighed. Aliphatic fractions were eluted using silica gel-alumina column chromatography with *n*-hexane.

GC-MS analyses for aliphatic fractions were carried out at the Key Laboratory of Petroleum Resources Research, Northwest Institute of Eco-Environment Resources, Chinese Academy of Sciences. The GC-MS analysis was performed using an HP 5973 MSD (Aglient Technologies, Wilmington, DE, United States) interfaced to an HP 6890 gas chromatograph that was fitted with a 30 m × 0.25 mm fused silica capillary column coated with a

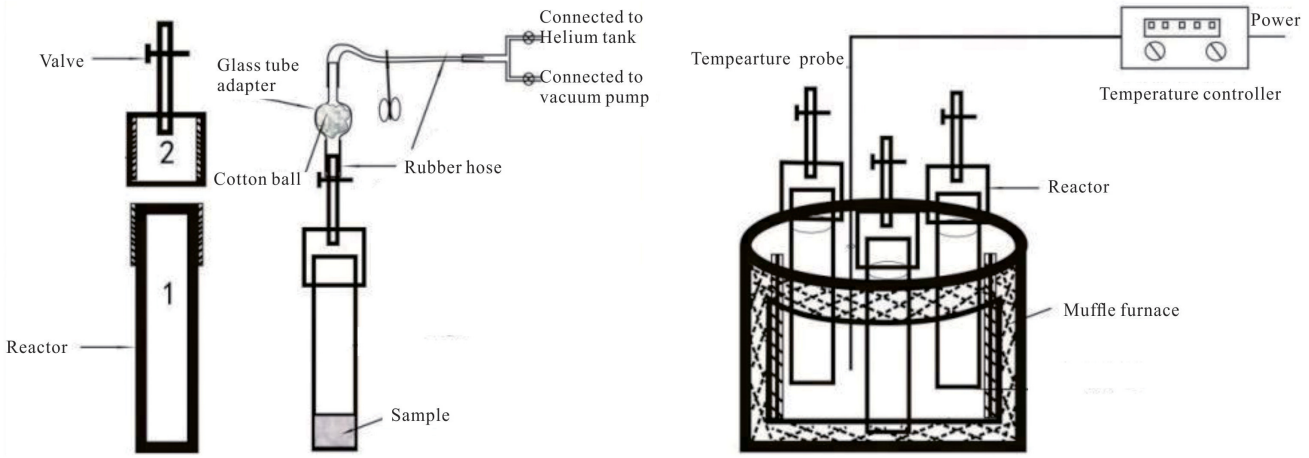

FIGURE 2 | Schematic diagram of the low-temperature thermal simulation experimental apparatus.

film (0.25 μm) of 5% phenyl-methyl. For routine GC analysis, the oven temperature was programmed to increase from 80 to 300°C at a rate of 3°C/min with a final hold time of 20 min. Helium was used as carrier gas at a linear velocity of 32 cm/s, with the injector operating at a constant flow of 0.9 ml/min. The MS was operated with an ionization energy of 70 eV, a source temperature of 230°C and an electron multiplier voltage of 1,900 V over the range of 35–550 Da. Prior to analyses, the GC-MS was tuned using perfluorotributylamine (PFTBA) and blank samples were applied to check the background.

Low Temperature Thermal Simulation Experiments and Analyses of Gas Composition and Compound-Specific Carbon Isotopes

The experiment was conducted in a self-designed simulation instrument. As shown in **Figure 2**, the device is comprised of a reactor with a volume of 300 ml, a ceramic fiber muffle furnace, and a high precision temperature controller (±1°C). Jiang and Song (1992) established the relationship between the simulated temperature and sediment vitrinite reflectance (Ro%) based on the thermal simulation experiments on immature source rocks from Junggar Basin, and indicated that the sediment samples were still in the immature-low mature stage, when the thermal simulation temperature was lower than 350°C. Additionally, previous studies by Zhang et al. (2001) and Xie et al. (2002) suggested that the peak amount of carbon gases generally produced between 300–400°C. Consequently, in the present study, the experiment temperature was set as 350°C, and experiment time was set for 72 h.

The generated gases were analyzed using the MAT 271 mass spectrometer (Finnigan AG) and Gas Chromatography (GC) 5890C (Agilent Technologies). Basically, the non-hydrocarbon gases and the hydrocarbon gases (C_1–C_3) were measured by MAT 271 and GC 5890C equipped with a capillary column (HT-PLOT Al_2O_3, 50 m × 0.53 mm × 25 μm), respectively. A flame ionization detector (FID) and thermal conductivity detector (TCD) were connected to the column using Helium as the carrier gas. The GC 5890C oven temperature was initially set to 50°C for 5 min, and then increased to 200°C at a rate of 6°C/min, finally maintained for 10 min.

The compound-specific carbon isotope values of CO_2 and hydrocarbon gases (C_1–C_3) were performed on a VG Isochrom II isotope ratio mass spectrometer (IRMS) interfaced with an HP 5890 GC, fitted with a Poraplot Q column (30 m × 0.32 mm). Helium was used as the carrier gas. The column head pressure was 0.58 bar. The GC oven temperature was initially held at 40°C for 3 min, ramped from 40 to 180°C at 20°C/min, and held at 180°C for 5 min. Carbon isotope ratios for individual gaseous hydrocarbon compounds were measured using CO_2 as a reference gas, which was automatically introduced into the IRMS at the beginning and end of each analysis. The carbon isotope value of the CO_2 reference gas was calibrated against NBS-22 oil. In addition, a standard mixture (NG3) of gaseous hydrocarbons (C_1–C_3), with known isotope compositions calibrated by our laboratory (**Table 2**, Dai et al., 2012), was used daily to check the performance of the instrument. The standard deviation for replicate analyses of this mixture is better than 0.3‰ for each compound.

RESULTS

Ro, TOC Contents and *n*-Alkane Distribution Patterns of Xiaolongtan Sediments

The Ro values of representative XLT-I and XLT-II sediments varied between 0.29% and 0.32, 0.36, and 0.39%, respectively, suggesting the sediments were in the stage of immature.

The TOC concentration for sediments of XLT-I section fluctuated from 0.05 to 28.56%, with an average of 4.61%. For the upper XLT-II section, the TOC was between 0.24 and 52.34%, with an average value of 24.42%.

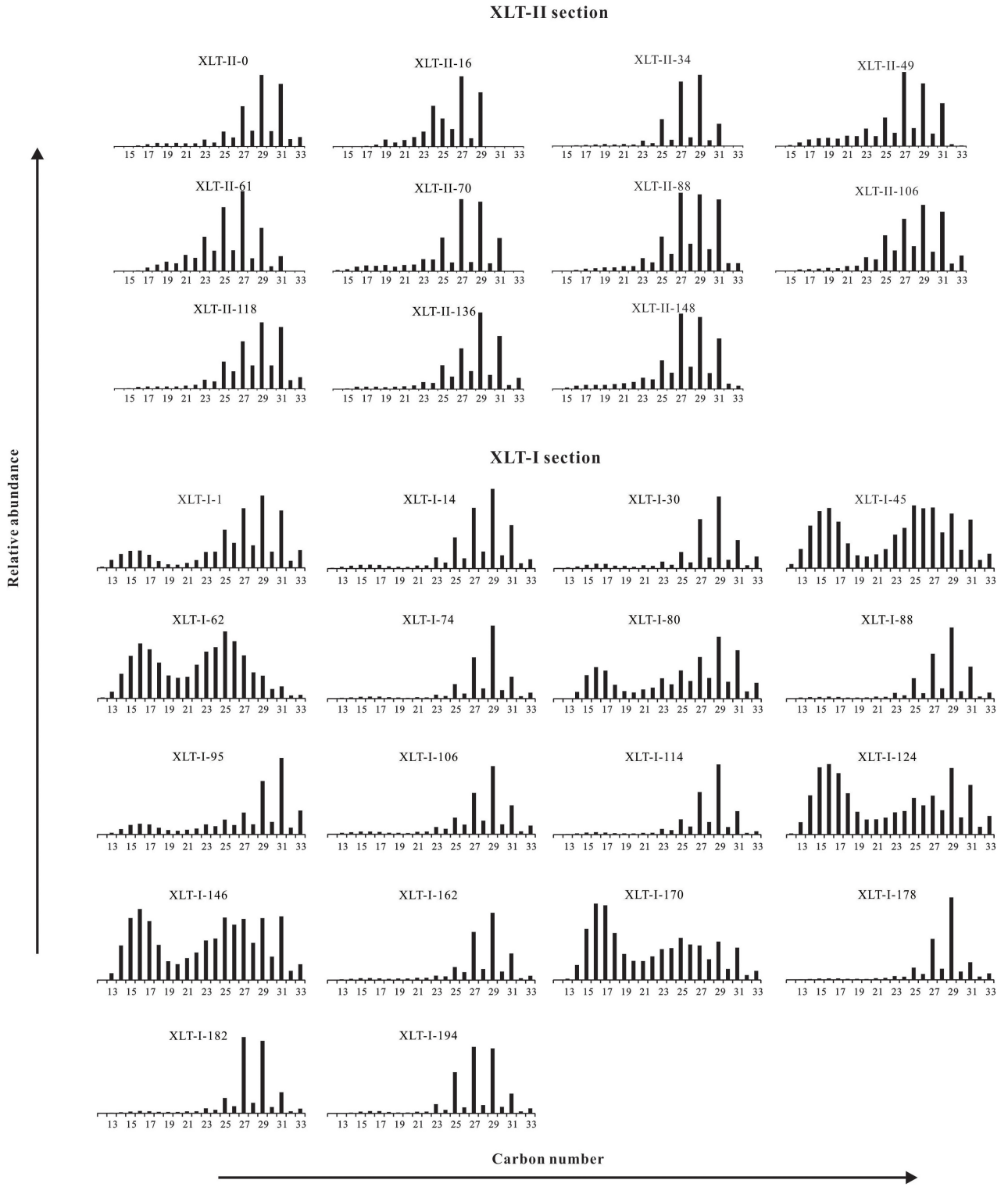

FIGURE 3 | Distribution patterns of *n*-alkanes of representative sediments from XLT-I and XLT-II sections.

The *n*-alkanes of the XLT-I section sediments ranged from nC_{12} to nC_{33}, with either a unimodal or bimodal distribution. The bimodal distribution of *n*-alkanes was centered on nC_{29}/nC_{31} and nC_{16}, generally. Whereas, the characteristic unimodal distribution of *n*-alkanes had a maximum carbon number at nC_{29}/nC_{31} (**Figure 3**). As for the *n*-alkane distribution

pattern of sediments from XLT-II section, it displayed a predominant back modal, ranging from nC_{14} to nC_{33}, with maxima at nC_{27}/nC_{29} (**Figure 3**). For the long-chain *n*-alkanes, a distinct odd-over-even predominance was observed throughout the sequence.

Production Rates of Generated Gases

The main components of the generated gases contained the non-hydrocarbon gases including CO_2, N_2 and H_2, accounting for the 89.0 ∼ 99.7% of the total gases, and the hydrocarbon gases including CH_4, C_2H_6 and C_3H_8, among which the CO_2 was the most abundant fraction ranging from 21.4 to 94.4% (**Table 1**). In terms of the hydrocarbon gases, the CH_4 was the most abundant.

Generally, the total gas production rate was estimated between 2,920 and 88,310 ml/kg rock, with an average value of 36,900 ml/kg rock. As for the carbon gases, the production rate was between 1,150 and 75,140 ml/kg rock for CO_2, 10 and 4,010 ml/kg rock for CH_4, and 20 and 5,890 ml/kg rock for total hydrocarbon gases (including CH_4, C_2H_6, and C_3H_8), with an average value of 31,910 ml/kg rock, 1,290 ml/kg rock and 1,940 ml/kg rock, respectively.

TABLE 1 | Contents of the CO_2, CH_4, and hydrocarbon gases (C_1–C_3) from the low temperature thermal simulation experiments.

Sample	Contents (%)		
	CO_2	CH_4	Hydrocarbon gases
XLT-I-148	90.7	3.0	4.3
XLT-I-136	87.4	3.2	4.9
XLT-I-118	77.2	5.1	7.3
XLT-I-106	88.0	2.9	5.4
XLT-I-88	88.7	3.2	4.9
XLT-I-70	85.7	3.9	5.5
XLT-I-49	87.0	4.2	5.9
XLT-I-34	83.7	4.2	6.2
XLT-I-16	85.1	3.2	4.9
XLT-I-0	82.1	5.4	7.9
XLT-II-194	93.6	2.7	3.9
XLT-II-182	94.4	2.4	3.1
XLT-II-178	92.1	3.4	4.7
XLT-II-170	90.1	0.4	0.6
XLT-II-162	88.6	0.3	0.5
XLT-II-146	75.4	5.3	11.0
XLT-II-124	94.1	0.2	0.3
XLT-II-114	86.2	2.9	5.7
XLT-II-106	61.9	4.2	8.3
XLT-II-95	21.4	1.2	2.2
XLT-II-88	73.2	5.5	9.3
XLT-II-80	90.7	0.7	1.2
XLT-II-74	87.0	4.8	6.6
XLT-II-62	78.4	0.2	0.3
XLT-II-45	46.8	0.6	0.9
XLT-II-30	94.3	1.8	3.0
XLT-II-14	83.1	4.6	9.6
XLT-II-1	79.5	0.7	1.7

Compound-Specific Carbon Isotopes of Carbon Gases

As listed in **Table 2**, the $\delta^{13}C$ values of CO_2 ranged from −24.8 to −16.0‰, with a mean value of −20.9‰. As for the hydrocarbon gases, the $\delta^{13}C$ values of CH_4, C_2H_6, and C_3H_8 fluctuated between −43.8 and −37.2‰, −34.2 and −32.1‰, −33.4 and −30.6‰, with an average of −40.2 −33.3, and −31.9‰, respectively. To be more specific, the $\delta^{13}C$ values of CH_4, C_2H_6, and C_3H_8 were characterized by normal isotope ordering, displaying $\delta^{13}C_{CH4} < \delta^{13}C_{C2H6} < \delta^{13}C_{C3H8}$.

DISCUSSION

Sources of Organic Matter and Paleoclimate Interpretation

In lacustrine environments, organic matter contains a wide range of lipid compounds contributed from autochthonous and/or heterochthonous organisms. Difference in lipid composition can directly reflect different types of biota (Pearson et al., 2007). Previous studies indicated that the short-chain *n*-alkanes ranging from C_{14} to C_{21} and dominated by C_{16} or C_{18}, are derived from lower organisms including algae, cyanobacteria, fungi, and microbes (Cranwell et al., 1987; Meyers and Ishiwatari, 1993). The middle-chain *n*-alkanes with carbon numbers in the range of C_{23} to C_{25} are thought to be from submerged/floating macrophytes (Ficken et al., 2000). By contrast, the long-chain *n*-alkanes ranging from C_{27} to C_{33}, showing an obvious odd-over-even predominance and dominated by C_{27}, C_{29}, C_{31} or C_{33}, are considered to come from terrestrial higher plants (Eglinton and Hamilton, 1967; Ficken et al., 2000).

TABLE 2 | Compound-specific carbon isotopes of the CH_4, C_2H_6, C_3H_8, and CO_2 of generated carbon gases from XLT-I and XLT-II sections.

Sample	$\delta^{13}C$ (‰)			
	CH_4	C_2H_6	C_3H_8	CO_2
XLT-I-148	−37.8	−33.4	−31.7	−21.7
XLT-I-118	−39.1	−32.9	−32.8	−21.2
XLT-I-88	−39.0	−33.6	−32.7	−23.3
XLT-I-34	−38.8	−32.6	−31.5	−20.8
XLT-I-0	−42.6	−33.2	−30.6	−21.5
XLT-II-182	−37.2	−32.8	−31.9	−23.5
XLT-II-170	–	–	–	−18.0
XLT-II-146	−42.1	−34.1	−31.5	−23.5
XLT-II-114	−40.0	−34.2	−32.8	−21.9
XLT-II-95	−40.9	−32.1	−30.8	−17.1
XLT-II-80	−43.6	−33.6	−33.4	−16.6
XLT-II-62	−43.8	–	–	−16.0
XLT-II-30	−39.8	−33.4	−30.9	−24.8
XLT-II-14	−37.7	−34.1	−32.4	−22.7
Standard sample	−43.6	−40.2	−33.8	–

"–" indicate the concentration of the corresponding gas component is too low to be measured, and the $\delta^{13}C$ values of CH_4, C_2H_6, and C_3H_8 of the standard sample (NG3) are from Dai et al. (2012).

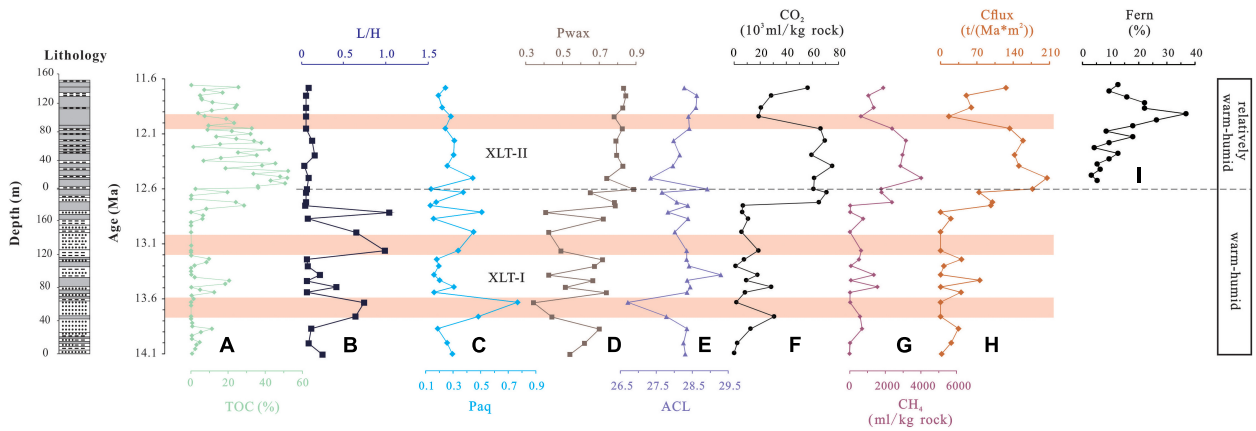

FIGURE 4 | Variations though time in various paleoenvironmental indicators for the Xiaolongtan Basin: **(A)** TOC contents, **(B)** L/H ratios, **(C)** Paq values, **(D)** Pwax values, **(E)** ACL values, **(F)** estimated production rate of CO_2, **(G)** estimated production rate of CH_4, **(H)** burial rate of organic carbon and **(I)** percentage of ferns in the Xiaolongtan Formation. Bars in this figure indicate three episodes of enhanced humidity inferred from lipid biomarkers and pollen concentrations.

The *n*-alkanes of XLT-I sediments were characterized by both bimodal and unimodal distribution patterns (**Figure 3**), indicating mixed sources of organic matter from lower organisms and terrestrial higher plants. With decreasing burial depths, the sources of organic matter shifted from mixed sources to terrestrial higher plants. Throughout the XLT-II section, all the *n*-alkanes displayed unimodal distribution centered at C_{27}, C_{29}, or C_{31} with a strong odd-over-even predominance (**Figure 3**), suggesting a primary contribution from terrestrial plants. The abundance of middle chain *n*-alkanes remained rather low, implying a very limited source from submerged/floating marcrophytes. Previous studies suggested that sediments with Pr/C_{17} and Ph/C_{18} ratios lower than 1, may go through weak microbial degradation (Grimalt et al., 1988; Gonzalez-Vilia et al., 2003; Wang et al., 2012). In most of our samples, the Pr/C_{17} and Ph/C_{18} ratios were lower than 1, implying that the middle chain *n*-alkanes were probably not affected by the microbial degradation (Grimalt et al., 1988; Gonzalez-Vilia et al., 2003; Wang et al., 2012). Thus, it is not likely that the long-chain *n*-alkanes were produced by emergent and submerged aquatic plants, although there are reports pointing out a few emergent and submerged plants can produce C_{27} or C_{29} *n*-alkanes (Aichner et al., 2010; Liu and Liu, 2016; Liu et al., 2016). In addition, the L/H ratio (calculated as $\Sigma nC_{21}^{-}/\Sigma nC_{22}^{+}$), which has been used to reflect the relative abundance of low molecular *n*-alkanes to high molecular homologs (Bai et al., 2006), ranged from 0.04 to 1.05, with an average value of 0.23 (**Figure 4B**), implying a significant contribution of terrestrial higher plants to the organic matter in the XLT-I and XLT-II sediments.

In addition, the XLT-I section is dominated by sandstone and clay intercalated with thin coal and marl layers, which may indicate delta plain and braided river facies (Zhang et al., 2019). Our results showed that the sedimentary organic matter was contributed by lower organisms and terrestrial higher plants, in accordance with the sedimentary environments. Furthermore, as indicated above, the *n*-alkane distribution patterns of XLT-II samples revealed a terrestrial plant contribution to the organic matter. The evidence from lithology and pollen assemblages implied the sedimentary environment of XLT-II section was interpreted as swamp face and the vegetation was dominated by angiosperms (Li S.F. et al., 2015; Zhang et al., 2019). Our *n*-alkane results were consistent with previous claims. Both the source of organic matter and the sedimentary environment favored the formation of lignite in this section.

Previous studies have indicated that the Paq [calculated as $(C_{23} + C_{25})/(C_{23} + C_{25} + C_{27} + C_{29})$] and Pwax [calculated as $(C_{27} + C_{29} + C_{31})/(C_{23} + C_{25} + C_{27} + C_{29} + C_{31})$] proxy can be applied to reflect the relative abundance of non-emergent aquatic marcophytes and input of emergent aquatic and terrestrial plants, and its corresponding paleoclimate conditions (Ficken et al., 2000; Zheng et al., 2007; Pu et al., 2011; Wang G. et al., 2019). A high Pwax value represents a high input of terrestrial plants from herbs and trees, which may indicate a warm climate with low precipitation, corresponding to a low Paq values (Zheng et al., 2007; Pu et al., 2011). Besides, the ACL [average chain length, calculated as $(25^{*}C_{25} + 27^{*}C_{27} + 29^{*}C_{29} + 31^{*}C_{31})/(C_{25} + C_{27} + C_{29} + C_{31})$] values of *n*-alkanes was proposed to be an effective index for evaluating the temperature variation (Poynter et al., 1989), which have been successfully applied in paleoclimate reconstruction in loess/paleosol and lake sediments (Zhang et al., 2006; Pu et al., 2011; Chu et al., 2014). Recent studies have revealed that vegetation types, effective precipitation, as well as biologic function of plant waxes also influence the ACL values (Schefuß et al., 2003; Bush and McInerney, 2015). Thus, the ACL values may represent a combined signal of these factors mentioned above. In our study, the ACL values displayed similar variation trends with the Pwax values and opposite changes with the Paq values, indicating that the ACL proxy contained the same paleoclimatic implications with Pwax, with higher values corresponding to warm and dry climate conditions.

For the XLT-I section between 14.1 and 12.6 Ma, the Pwax and Paq values remained relatively unstable, indicating the source

of organic matter varied accordingly. The relatively low Paq and high ACL values implied that this stage was generally characterized by a warm and humid but unstable climate (**Figure 4**). Based on the lithology with coal representing swamps with dense trees or grasses and marl denoting shallow lakes with evaporative carbonates, Zhang et al. (2019) inferred that the XLT-I sediments can be indicators of forest steppe in a subtropical warm and humid monsoon climate from 14.1 to 12.6 Ma. Previous studies indicated that the significant tectonic activity of the entire Tibetan Plateau at ∼14 Ma was responsible for the differences in aridity in the southeastern Tibetan Plateau during the middle-late Miocene, which was characterized with dry conditions in the western high-elevation regions and relatively humid environment in the eastern low-elevation areas under the background of equal supply of moisture from the Indian monsoon (Jacques et al., 2011), and the differences of flora in the north-south transition displaying evergreen broad-leaved forest in the subtropical areas and taxa in the tropical regions in the late Miocene (Jacques et al., 2014). These observations lead to the argument that the climate during the period between 14.1 and 12.6 Ma was strongly affected by both the evolution of the Indian monsoon and the uplift of the southeaster Tibetan Plateau (Wang et al., 1998; Huang et al., 2007; Zhang et al., 2019). Interestingly, the Pwax values displayed a sharp decrease in the episodes at around 13.8–13.5 Ma and 13.1–12.9 Ma, and the Paq values exhibited the opposite variation, suggesting an enhanced input of aquatic macrophytes during these two intervals, probably in response to the increased precipitation/runoff. During these two intervals, the climate became more humid than before, in concert with the sediment environment shifting from delta plain toward braided river (Zhang et al., 2019). Variations in the hydrodynamic forces may cause changes in the transportation and the later accumulation and deposition of organic matter. This was further corroborated by the varying and low TOC contents (**Figure 4A**).

For the XLT-II section between 12.6 and 11.6 Ma, the *n*-alkane distribution patterns indicated a constant contribution from terrestrial plants, which was further supported by the high Pwax and low Paq proxies (**Figure 4**), implying this interval was characterized by warm but less wet climate conditions. The ACL values displayed an overall increasing trend, suggesting a slight increase of aridity. The results were consistent with the sedimentary facies changing to swamp, and the ecological environment shifting from forest steppe to forest (Zhang et al., 2019). The pollen assemblages found in the XLT-II section were dominated by angiosperms which represent the evergreen broad-leaved forests, such as *Cupuliferoipollenites, Cyrillaceaepollenites, Liquidambarpollenites, Caryapollenites, Salixipollenites, Ilexpollenites, Rutaceoipollis, Juglanspollenites, Talisiipites, Platycaryapollenites* (Wang, 1996; Li S.F. et al., 2015). Moreover, the mammal fossils of arboreal primate hominoids and forest elephants in the Xiaolongtan Basin also indicated a warm and relatively humid climate suitable for the survival of these mammals (Dong, 1987, 2001). During this stage, the warm and less humid climate and stable sedimentary environment benefited the formation, accumulation and deposition of organic matter, leading to the high TOC concentrations of the XLT-II section sediments. Overall, slight increases in arid conditions between 12.6 and 11.6 Ma were superimposed on long-term warm and humid climate.

Carbon Gas Behaviors Associated With Paleoclimate Conditions

The production rate of CO_2 and CH_4 displayed significantly positive correlation with the TOC contents of sediment, with r^2 values of 0.85 and 0.91, respectively (**Figures 5A,B**), indicating the carbon gases were mainly generated from the organic matter. Additionally, the $\delta^{13}C$ values of CH_4, C_2H_6, and C_3H_8 exhibited a normal isotope ordering (**Figure 5E**), and the $\delta^{13}C$ values of CO_2 were lower than $-10‰$, suggesting organic origin of the generated carbon gases (Dai et al., 1996, 2005). Consequently, it is reasonable to infer that the CO_2 and hydrocarbon gases including CH_4, C_2H_6, and C_3H_8 were produced by thermal effect of sedimentary organic matters during their shallow burial process.

Basically, the production rate of carbon gases was primarily controlled by the sedimentary TOC content, showing high production rates of both CO_2 and hydrocarbon gases in response to high sediment TOC concentration. In the XLT-I sediments, the production rate of carbon gases was lower than that of the XLT-II sediments, mainly due to the significant differences of TOC contents of sediments from the two sections. In addition, both the CO_2 and CH_4 (and hydrocarbon gases) production rate displayed weak positive correlations with the Pwax values (**Figures 5C,D**), with r^2 values of 0.48 and 0.52, respectively, indicating that warm and dry climate conditions may be favorable of the formation of carbon gases. Our results suggested that the paleoclimate conditions played an important role in the generation of carbon gases. Particularly, in the XLT-I section, the production rate of carbon gases showed an obvious decrease when the climate shifted toward more humid conditions at around 13.8 ∼ 13.5 Ma and 13.1 ∼ 12.9 Ma. Thereafter, under the background of long-term warm and humid climate conditions, with the increase of aridity, both the CO_2 and hydrocarbon gases production rate rose correspondingly. In the XLT-II section, the sedimentary environment changed to swamp (Zhang et al., 2019), which favored formation, accumulation and deposition of organic matter, resulting in high sedimentary TOC concentrations. The warm and relatively dry climate also benefited the generation of carbon gases during that time. Generally, the average production rate of CO_2 and CH_4 was 2 ∼ 3 times larger than that of the XLT-I section. The pollen records indicated this interval was warm and humid. However, the abundance of ferns and angiosperms exhibited variations, implying variations in humidity and temperature. The production rate of CO_2 and CH_4 showed a negative correlation with the abundance of fern (**Figure 4**), exhibiting high production rates corresponding to low abundance of ferns. Both the CO_2 and CH_4 production rate increased and stayed high from 12.6 to 12.0 Ma, in line with the low fern percentage. However, the gas production rate decreased after 12.0 Ma, in accordance with the sharp rise in the abundance of ferns. Interestingly, a slight increase of Paq value and corresponding decrease of Pwax value at around 12.0 Ma indicated an increase in humidity. In addition, the gradual

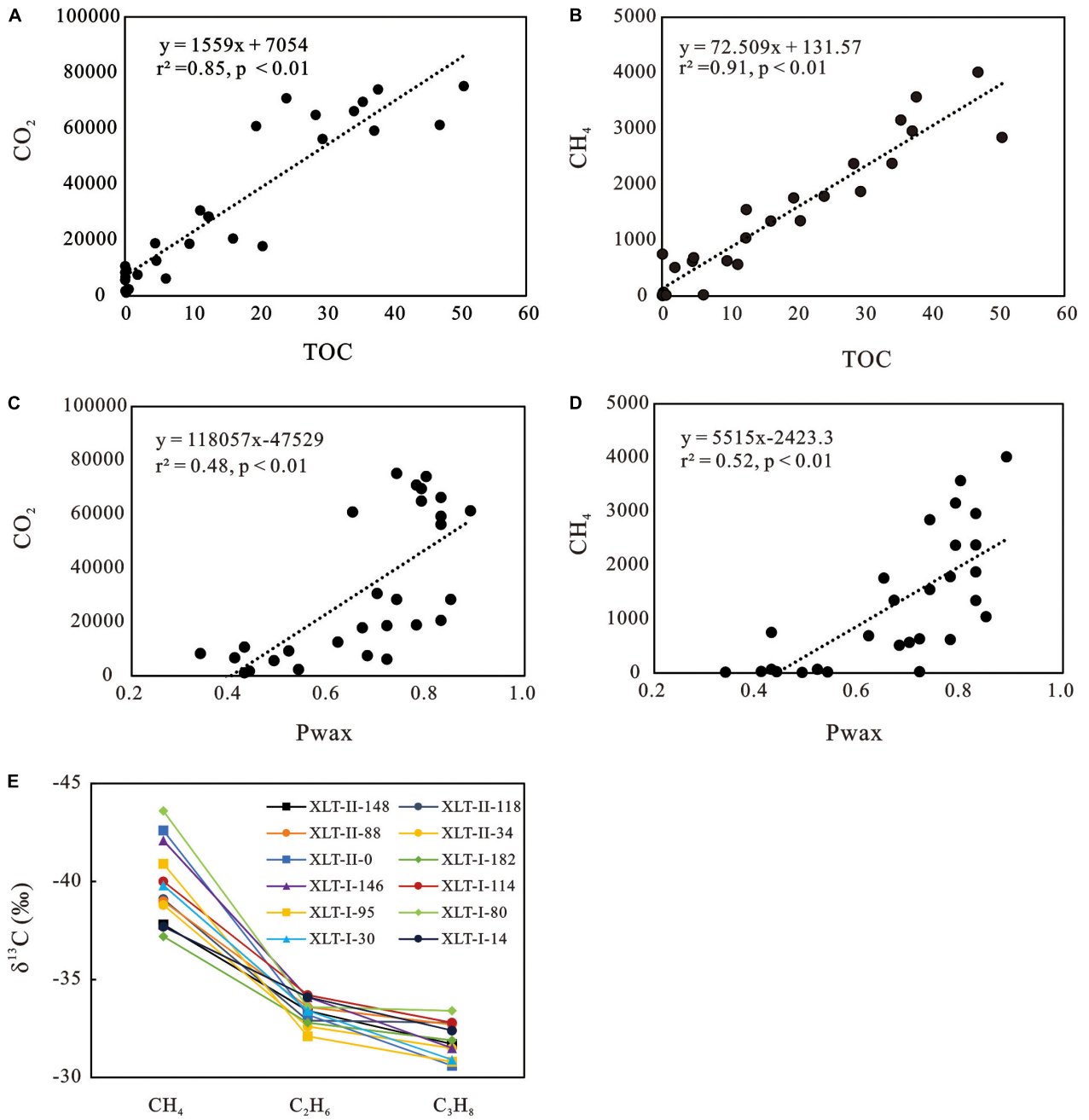

FIGURE 5 | Correlations between TOC contents and production rate of CO_2 and CH_4 **(A,B)**, and Pwax values and production rate of CO_2 and CH_4 **(C,D)**, and compound-specific carbon isotopes of CH_4, C_2H_6 and C_3H_8, respectively **(E)**.

changes of sedimentary facies to shallow lakes at the upper part of XLT-II section as a result of compressive uplift (Dong, 2001; Zhang et al., 2019), also implied that the increase in humidity was probably related to enhanced precipitation, leading to unstable hydrodynamic environment for accumulation and deposition of organic matter, and consequent low carbon gas production rate.

In summary, our results indicated that the carbon gases can be produced during the shallow burial process when the sediments reached appropriate conditions of pressure and temperature. From 14.1 to 11.6 Ma, the production rate of carbon gases displayed significant variations in response to the fluctuations of paleoclimate conditions, which was regulated by the variations of the Indian monsoon and the uplift of the Tibetan Plateau. Generally, warm and less humid climate was conducive to the formation, accumulation and deposition of organic matter, which acted as the material basis for the generation of carbon gases. The low gas production rate corresponded with increased humidity,

indicating that warm and less humid (arid) climate contributed to the thermal effects of organic matter to transform to carbon gases.

Original Organic Carbon Burial Rates

The low-temperature thermal simulation experiments showed that when reaching appropriate temperature and pressure, the organic matter would go through the thermodynamic effect to produce carbon gases during their shallow burial process, resulting in changes of the TOC contents of sediments. Therefore, in order to achieve the original signal of organic carbon concentration, it is important to restore the sediment TOC. Combining the efforts of geologic observation, experimental simulation and numerical modeling, Zhong et al. (2004) proposed a method to evaluate variations of sediment TOC contents during their geological history, and established an equation to estimate the loss of TOC when undergoing thermal maturation.

For the XLT-1 and XLT-II section simulated sediments, the TOC contents varied between 0.05 and 50.70% (**Table 3**). The TOC contents of the samples after thermal simulation experiments (expressed as TOC*) fluctuated from 0.07 to 44.20%. The overall trend exhibited that the TOC contents of sediment decreased after experiments. The loss ratio of TOC (expressed as DTOC) varied in the range from −0.83 to 0.34, and the corresponding calculated recovery coefficients (k) fluctuated between 0.55 and 1.51. The restored TOC (expressed as TOC°) representing the original TOC varied between 0.03 and 58.16% (**Table 3**), further confirming that most of the original sedimentary TOC decreased after the burial process.

It should be pointed out that some of the sediments characterized by low TOC concentrations especially for the XLT-I section (such as samples XLT-I-45, XLT-I-62, XLT-I-80, XLT-I-95, XLT-I-124, XLT-146, and XLT-I-170) displayed a "carbon addition" phenomenon, which revealed during the sediment thermal maturation process, little carbon gases were produced by the organic matter and a certain amount of inorganic sediments consumed. So after restoration, the original TOC (TOC°) displayed slightly higher values than that of the present sediments. By contrast, the rest part of the sediments with high TOC contents were characterized by "carbon reduction," indicating a certain amount of organic matter was transformed to carbon gases.

Based on the restoration of TOC, we estimated the original organic carbon burial rate (expressed as C_{flux}) in the study area. Previous studies indicated that the organic carbon burial rate can be calculated using the following equation, expressed as C_{flux} = TOC × ν × ρ, where ν represents the sedimentation rate, and ρ represents the dry density of the sediments (Xu et al., 2013; Ruiz-Fernández et al., 2018). Generally, the organic carbon burial rate varied from 0.1 to 205.1 t/(m^2·Ma), with an average value of 60.0 t/(m^2·Ma), characterized by far more larger values in the XLT-II section sediments than that of the XLT-I sediments (**Figure 4G**). Generally, under the background of persistent warm and humid climate conditions, our estimated burial rate of organic carbon was mainly controlled by the primary production, which regulated the input of organic matter. Besides, the higher sedimentation rates in the XLT-II sediments also elevated the burial efficiency and preservation of organic matter (Makled et al., 2019). Similar with the estimations of gas production rate, the burial rate of organic carbon corresponded well with the paleoclimate conditions as indicated by the lipid biomarkers, pollen assemblages and lithology (Zhang et al., 2019), showing decreasing trend when climate became wetter.

Quantification of carbon burial of Qinghai Lake sediments by Xu et al. (2013) indicated that TOC flux was higher during the warm and wet periods than in the cold and dry episodes. Besides, based on the studies of 42 lakes across China, Zhang et al. (2013) claimed that the burial rate of organic carbon during the Holocene climatic optimum was higher than in modern times, due to the warm and humid climate, enhanced input of organic matter and high primary productivity in lakes. In the present study, the warm and humid climate and the generally reducing sedimentary environment as reflected by the Pr/Ph proxy (ranging from 0.31 to 1.40, average 0.98) favored the formation, deposition, and preservation of organic matter, resulting in

TABLE 3 | Total organic carbon (TOC) restoration parameters of Xiaolongtan Basin sediments.

Sample	TOC (%)	TOC* (%)	DTOC	*k*	TOC° (%)
XLT-II-148	29.60	24.50	0.17	1.21	35.76
XLT-II-136	12.50	11.10	0.11	1.13	14.08
XLT-II-118	16.20	15.60	0.04	1.04	16.82
XLT-II-106	4.50	4.40	0.02	1.02	4.60
XLT-II-88	34.30	31.10	0.09	1.10	37.83
XLT-II-70	35.60	28.10	0.21	1.27	45.10
XLT-II-49	37.90	35.50	0.06	1.07	40.46
XLT-II-34	37.30	32.50	0.13	1.15	42.81
XLT-II-16	50.70	44.20	0.13	1.15	58.16
XLT-II-0	47.10	44.20	0.06	1.07	50.19
XLT-I-194	19.64	15.00	0.24	1.31	25.72
XLT-I-182	24.18	16.90	0.30	1.43	34.60
XLT-I-178	28.56	24.30	0.15	1.18	33.57
XLT-I-170	0.08	0.14	−0.75	0.57	0.05
XLT-I-162	6.15	5.49	0.11	1.12	6.89
XLT-I-146	0.05	0.07	−0.40	0.71	0.04
XLT-I-124	0.07	0.11	−0.57	0.64	0.04
XLT-I-114	9.67	6.67	0.31	1.45	14.02
XLT-I-106	1.90	1.58	0.17	1.20	2.28
XLT-I-95	0.20	0.33	−0.65	0.61	0.12
XLT-I-88	20.61	16.25	0.21	1.27	26.14
XLT-I-80	0.24	0.34	−0.42	0.71	0.17
XLT-I-74	12.55	11.50	0.08	1.09	13.70
XLT-I-62	0.06	0.11	−0.83	0.55	0.03
XLT-I-45	0.08	0.12	−0.50	0.67	0.05
XLT-I-30	11.29	10.70	0.05	1.06	11.91
XLT-I-14	4.72	3.13	0.34	1.51	7.12
XLT-I-1	0.59	0.46	0.22	1.28	0.76

TOC refers to the TOC contents of present sediments; TOC refers to the TOC contents of samples after thermal simulation experiments; DTOC refers to the loss factor of organic carbon; k refers to the recovery coefficient; TOC° refers to the original TOC contents of the sediments after the restoration estimated according to the method proposed by Zhong et al. (2004).*

DTOC = (TOC − TOC)/TOC*; k = 1/(1 − DTOC); TOC° = TOC × 1/(1 − DTOC).*

relatively high sediment TOC concentrations, and consequently high organic carbon burial rate. Particularly, the low burial rates acted in response to the sharp increase of humidity. For example, during the period of 13.8–13.5 Ma and 13.1–12.9 Ma, the climate was wetter than before. And correspondingly, the burial rate of organic carbon was extremely low, ranging from 0.09 to 0.14 t/(m^2·Ma). Furthermore, the minimum value of organic carbon burial rate at around 12.0 Ma in the XLT-II section also corresponded to the climate becoming wetter.

Generally, the average burial rate of organic carbon in the XLT-I and XLT-II sections was estimated to be 60.0 t/(m^2·Ma), which is larger than 43.2 and 36.4 g/(m^2·a) from the lake sediments in the East China, 50.9 and 22.1 g/(m^2·a) from the lakes in the Inner Mongolia and Xinjiang, 33.5 and 19.7 g/(m^2·a) from the lake records in the Qinghai-Tibetan Plateau, and 22.0 and 16.6 g/(m^2·a) from the lake sediments in the Yunnan–Guizhou Plateau during the Holocene climatic optimum and modern times (Zhang et al., 2013). Our results indicated that the Xiaolongtan Basin might have been a sink for organic carbon between 14.1 and 11.6 Ma. After the sequestration of organic carbon, this carbon pool probably acted as a source for the carbon gases produced by thermal effects during the shallow burial process.

CONCLUSION

Based on the precise chronological framework, analyses of lipid biomarkers and low temperature thermal simulation experiments were carried out from the Xiaolongtan Basin in the southeastern part of the Tibetan Plateau. The preliminary conclusions drawn from this study were listed below:

(1) According to the characteristics of *n*-alkanes and its derived proxies (including Paq and Pwax), it is indicated that the organic matter of the XLT-I sediments was mainly derived from mixed sources including lower organisms and terrestrial higher plants, and terrestrial higher plants primarily contributed to the XLT-II sediments.
(2) As reflected by the lipid biomarkers and pollen records, the climate between 14.1 and 12.6 Ma was warm and humid, and humidity slightly decreased between 12.6 and 11.6 Ma. And the climate was under the influence of both the evolution of Indian monsoon and the uplift of the southeastern Tibetan Plateau.
(3) The low temperature thermal simulation experiments showed that a certain amount of carbon gases (CO_2 and CH_4) can be produced and released into atmosphere owing to thermodynamic effects of organic matter during the shallow burial process. Original accumulation, deposition and preservation of organic matter primarily influenced the production rate of carbon gases and burial rate of organic carbon. Besides, the estimated production rate of carbon gases and burial rate of organic carbon displayed similar variation trends throughout the sequence, generally exhibiting decreasing trends in accordance with strengthened humidity, which was further controlled by the paleoclimate variations forced by the changes of Indian monsoon and the uplift of the Tibetan Plateau.

DATA AVAILABILITY STATEMENT

The original contributions generated for this study are included in the article/supplementary material, further inquiries can be directed to the corresponding author.

AUTHOR CONTRIBUTIONS

GW, YW, and ZW contributed conception and design of the study. GW and ZS executed the thermal simulation experiments. WH and XM carried out chemical analysis. GW wrote the first draft of the manuscript. All authors contributed to the article and approved the submitted version.

FUNDING

This work was financially supported by the National Natural Science Foundation of China (Grant Nos. 41831176, 41902028, and 41972030), the Second Tibetan Plateau Scientific Expedition and Research (STEP) Program (Grant No. 2019QZKK0707), the Chinese Academy of Sciences Key Project (Grant No. XDB26020302), the CAS 'Light of West China' Program, the Youth Innovation Promotion Association CAS (No. 2021425), and the Key Laboratory Project of Gansu (Grant No. 1309RTSA041).

ACKNOWLEDGMENTS

The authors show special thanks to the reviewers for their constructive comments and improvements of the language.

REFERENCES

Aichner, B., Herzschuh, U., and Wilkes, H. (2010). Influence of aquatic macrophytes on the stable carbon isotopic signatures of sedimentary organic matter in lakes on the Tibetan Plateau. *Org. Geochem.* 41, 706–718. doi: 10.1016/j.orggeochem.2010.02.002

Bai, Y., Fang, X. M., Wang, Y. L., Fabien, K., Chen, X. L., and Wang, Y. X. (2006). Branched alkanes with quaternary carbon atoms in Chinese soils: potential environmental implications. *Sci. Bull.* 51, 1115–1122. doi: 10.1007/s11434-006-1115-3

Bush, R. T., and McInerney, F. A. (2015). Influence of temperature and C4 abundance on n-alkane chain length distributions across the central USA. *Org. Geochem.* 79, 65–73. doi: 10.1016/j.orggeochem.2014.12.003

Choi, Y., and Wang, Y. (2004). Dynamics of carbon sequestration in a coastal wetland using radiocarbon measurements, global biogeochem. *Cycles* 18:GB4016.

Chu, G. Q., Sun, Q., Xie, M. M., Lin, Y., Shang, W. Y., and Zhu, Q. Z. (2014). Holocene cyclic climatic variations and the role of the Pacific Ocean as recorded in varved sediments from northeastern China. *Quat. Sci. Rev.* 102, 85–95. doi: 10.1016/j.quascirev.2014.08.008

Cranwell, P. A., Eglinton, G., and Robinson, N. (1987). Lipids of aquatic organisms as potential contributors to lacustrine sediments—II. *Org. Geochem.* 11, 513–527. doi: 10.1016/0146-6380(87)90007-6

Dai, J., Chen, H., and Shen, X. (2005). Geochemistry and occurrence of inorganic gas accumulations in Chinese sedimentary basins. *Org. Geochem.* 36, 1664–1688. doi: 10.1016/j.orggeochem.2005.08.007

Dai, J., Song, Y., Dai, C., and Wang, D. (1996). Geochemistry and accumulation of carbon dioxide gases in China. *AAPG Bull.* 10, 1615–1626.

Dai, J., Xia, X. Y., Li, Z. S., Coleman, D. D., Dias, R. F., Gao, L., et al. (2012). Inter-laboratory calibration of natural gas round robins for δ2H and δ13C using off-line and on-line techniques. *Chem. Geol.* 310-311, 49–55. doi: 10.1016/j.chemgeo.2012.03.008

Dong, W. (1987). Further investigations upon the age and characteristics of the Xiaolongtan fauna, Kaiyuan Co., Yunnan Province. *Vertebrata PalAsiatica* 25, 116–123.

Dong, W. (2001). "Upper Cenozoic stratigraphy and paleoenvironment of Xiaolongtan Basin, Kaiyuan, Yunnan Province," in *Proceedings of the Eighth Annual Meeting of the Chinese Society of Vertebrate Paleontology*, eds T. Deng and Y. Wang (Beijing: China Ocean Press).

Eglinton, G., and Hamilton, R. J. (1967). Leaf epicuticular waxes. *Science* 156, 1322–1335. doi: 10.1126/science.156.3780.1322

Fang, J. Y., Yu, G. R., Liu, L. L., Hu, S. J., and Stuart Chapin, F. (2018). Climate change, human impacts, and carbon sequestration in China. *Proc. Natl. Acad. Sci. USA* 115, 4015–4020.

Ficken, K. J., Li, B., Swain, D. L., and Eglinton, G. (2000). An n-alkane proxy for the sedimentary input of submerged/floating freshwater aquatic macrophytes. *Org. Geochem.* 31, 745–749. doi: 10.1016/s0146-6380(00)00081-4

Gao, Y., Huang, H., Tao, H. F., Carroll, A. R., Qin, J. M., Chen, J. Q., et al. (2019). Paleoenvironmental setting, mechanism and consequence of massive organic carbon burial in the Permian Junggar Basin, NW China. *J. Asian Earth Sci.* 194:104222. doi: 10.1016/j.jseaes.2019.104222

Gonzalez-Vilia, F. J., Polvillo, O., Boski, T., Moura, D., and de Andres, J. R. (2003). Biomarker patterns in a time-resolved holocene/terminal Pleistocene sedimentary sequence from the Guadiana river estuarine area (SW Portugal/Spain border). *Org. Geochem.* 34, 1601–1613. doi: 10.1016/j.orggeochem.2003.08.006

Grimalt, J. O., Torras, E., and Albaiges, J. (1988). Bacterial reworking of sedimentary lipids during sample storage. *Org. Geochem.* 13, 741–746. doi: 10.1016/0146-6380(88)90096-4

Heimann, M., and Reichstein, M. (2008). Terrestrial ecosystem carbon dynamics and climate feedbacks. *Nature* 451, 289–292. doi: 10.1038/nature06591

Huang, Y. J., Jia, L. B., Wang, Q., Mosbrugger, V., Utescher, T., Su, T., et al. (2016). Cenozoic plant diversity of Yunnan: a review. *Plant Diversity* 38, 271–282. doi: 10.1016/j.pld.2016.11.004

Huang, Y. S., Clemens, S. C., Liu, W. G., Wang, Y., and Prell, W. L. (2007). Large-scale hydrological change drove the late Miocene C4 plant expansion in the Himalayan foreland and Arabian Peninsula. *Geology* 6, 531–534. doi: 10.1130/g23666a.1

Jacques, F., Guo, S. X., Su, T., Xing, Y. W., Huang, Y. J., Liu, Y. S., et al. (2011). Quantitative reconstruction of the Late Miocene monsoon climates of southwest China: a case study of the Lincang flora from Yunnan Province. *Palaeogeogr. Palaeoclimatol. Palaeoecol.* 304, 318–327. doi: 10.1016/j.palaeo.2010.04.014

Jacques, F., Su, T., Spicer, R. A., Xing, Y. W., Huang, Y. J., and Zhou, Z. K. (2014). Late Miocene southwestern Chinese floristic diversity shaped by the southeastern uplift of the Tibetan Plateau. *Palaeogeogr. Palaeoclimatol. Palaeoecol.* 411, 208–215. doi: 10.1016/j.palaeo.2014.05.041

Ji, X. P., Jablonski, N. G., Su, D. F., Deng, C. L., Flynn, L. J., You, Y., et al. (2013). Juvenile hominoid cranium from the terminal Miocene of Yunnan, China. *Chin. Sci. Bull.* 58, 3771–3779. doi: 10.1007/s11434-013-6021-x

Jiang, S. B., and Song, Z. Y. (1992). Thermal modelling and gas yield potential analysis of gas source rocks in Junggar Basin. *Xinjiang Petroleum Geol.* 13, 86–93.

Li, S. F., Mao, L. M., Spicer, R. A., Lebreton-Anberrée, J., Su, T., Sun, M., et al. (2015). Late Miocene vegetation dynamics under monsoonal climate in southwestern China. *Palaeogeogr. Palaeoclimatol. Palaeoecol.* 425, 14–40. doi: 10.1016/j.palaeo.2015.02.030

Li, S. H., Deng, C. L., Dong, W., Sun, L., Liu, S. Z., Qin, H. F., et al. (2015). Magnetostratigraphy of the Xiaolongtan formation bearing *Lufengpithecus keiyuanensis* in Yunnan, southwestern China: constraint on the initiation time of the southern segment of the Xianshuihe–Xiaojiang fault. *Tectonophysics* 655, 213–226. doi: 10.1016/j.tecto.2015.06.002

Liu, H., and Liu, W. G. (2016). n-Alkane distributions and concentrations in algae, submerged plants and terrestrial plants from the Qinghai-Tibetan Plateau. *Org. Geochem.* 99, 10–22. doi: 10.1016/j.orggeochem.2016.06.003

Liu, W. G., Yang, H., Wang, H. Y., Yao, Y., Wang, Z., and Cao, Y. N. (2016). Influence of aquatic plants on the hydrogen isotope composition of sedimentary long-chain n-alkanes in the Lake Qinghai region, Qinghai-Tibetan Plateau. *Sci. China Earth Sci.* 59, 1368–1377. doi: 10.1007/s11430-016-5263-2

Makled, W. A., Abd, El Ghany, A. A., and Soliman, S. I. (2019). Tracking the key parameters stimulating organic carbon productivity, accumulation rate and preservation based on foraminiferal proxies in the subsurface Miocene sediments in north Sinai. *Egypt. Mar. Petrol. Geol.* 110, 218–239. doi: 10.1016/j.marpetgeo.2019.07.010

Meyers, P. A., and Ishiwatari, R. (1993). Lacustrine organic geochemistry - an overview of indicators of organic matter sources and diagenesis in lake sediments. *Org. Geochem.* 20, 867–900. doi: 10.1016/0146-6380(93)90100-p

Owens, J. D., Lyons, T. W., and Lowery, C. M. (2018). Quantifying the missing sink for global organic carbon burial during a cretaceous oceanic anoxic event. *Earth Planet. Sci. Lett.* 499, 83–94. doi: 10.1016/j.epsl.2018.07.021

Pearson, E. J., Farrimond, P., and Juggins, S. (2007). Lipid geochemistry of lake sediments from semi-arid Spain: relationships with source inputs and environmental factors. *Org. Geochem.* 38, 1169–1195. doi: 10.1016/j.orggeochem.2007.02.007

Poynter, J., Farrimond, P., Robinson, N., and Eglinton, G. (1989). *Aeolian-Derived Higher Plant Lipids in the Marine Sedimentary Record: Links with Palaeoclimate, Paleoclimatology and Paleometeorology: Modern and Past Patterns of Global Atmospheric Transport*. Berlin: Springer, 435–462.

Pu, Y., Zhang, H. C., Wang, Y. L., Lei, G. L., Nace, T., and Zhang, S. P. (2011). Climatic and environmental implications from n-alkanes in glacially eroded lake sediments in Tibetan Plateau: an example from Ximen Co. *Chin. Sci. Bull.* 56, 1503–1510. doi: 10.1007/s11434-011-4454-7

Ruiz-Fernández, A. C., Carnero-Bravo, V., Sanchez-Cabeza, J. A., Pérez-Bernal, L. H., Amaya-Monterrosa, O. A., Bojórquez-Sánchez, S., et al. (2018). Carbon burial and storage in tropical salt marshes under the influence of sea level rise. *Sci. Total Environ.* 630, 1628–1640. doi: 10.1016/j.scitotenv.2018.02.246

Schefuß, E., Ratmeyer, V., Stuut, J. B. W., Janse, J. H. F., and Damste, J. S. S. (2003). Carbon isotope analyses of n-alkanes in dust from the lower atmosphere over the central eastern Atlantic. *Geochim. Cosmochim. Acta* 67, 1757–1767. doi: 10.1016/s0016-7037(02)01414-x

Shao, H. B., Yang, S. Y., Cai, F., Li, C., Liang, J., Li, Q., et al. (2016). Sources and burial of organic carbon in the middle Okinawa trough during late quaternary paleoenvironmental change. *Deep Sea Res. 1 Oceanogr. Res. Papers* 118, 46–56. doi: 10.1016/j.dsr.2016.10.005

Smoak, J. M., Breithaupt, J. L., Smith, T. J., and Sanders, C. J. (2013). Sediment accretion and organic carbon burial relative to sea-level rise and storm events in two mangrove forests in everglades national park. *Catena* 104, 58–66. doi: 10.1016/j.catena.2012.10.009

Tapponnier, P., Xu, Z. Q., Roger, F., Meyer, B., Arnaud, N., Wittlinger, G., et al. (2001). Oblique stepwise rise and growth of the Tibet plateau. *Science* 294, 1671–1677. doi: 10.1126/science.105978

Wang, E., Burchfiel, B. C., Royden, L. H., Chen, L. Z., Chen, J. S., Li, W. X., et al. (1998). Late cenozoic xianshuihe-xiaojiang, red river, and dali fault systems of southwestern sichuan and central yunnan. *China Geol. Soc. Am. Bull.* 327, 1–108.

Wang, G., Wang, Y. L., Wei, Z. F., He, W., Ma, X. Y., Sun, Z. P., et al. (2019). Paleoclimate changes of the past 30 cal ka BP inferred from lipid biomarkers and geochemical records from Qionghai Lake, southwest China. *J. Asian Earth Sci.* 172, 346–358. doi: 10.1016/j.jseaes.2018.09.019

Wang, K., Zhang, H. S., Han, X. B., and Qiu, W. X. (2019). Sources and burial fluxes of sedimentary organic carbon in the northern Bering sea and the northern Chukchi sea in response to global warming. *Sci. Total Environ.* 679, 97–105. doi: 10.1016/j.scitotenv.2019.04.374

Wang, W. M. (1996). A palynological survey of neogene strara in xiaolongtan basin, yunnan province of south China. *Acta Geol. Sin.* 38, 743–748.

Wang, Y. L., Fang, X. M., Zhang, T. W., Li, Y. M., Wu, Y. Q., He, D. X., et al. (2012). Distribution of biomarkers in lacustrine sediments of the Linxia Basin, NE Tibetan Plateau, NW China: significance for climate change. *Seiment. Geol.* 243-244, 108–116. doi: 10.1016/j.sedgeo.2011.10.006

Wilson, R. M., Neumann, R. B., Crossen, K. B., Raab, N. M., Hodgkins, S. B., Saleska, S. R., et al. (2019). Microbial community analyses inform geochemical reaction network models for predicting pathways of greenhouse gas production. *Front. Earth Sci.* 7:59.

Woo, J. K. (1987). A revision of the classification of the Lufeng great ape. *Acta Anthropol. Sinica* 6, 265–271.

Xie, Z. Y., Jiang, Z. S., Zhang, Y., Li, J., Hu, G. Y., Wang, C. Y., et al. (2002). Novel method of whole rock pyrolysis and application to the evaluation of source rock. *Acta Sedimentologica Sinica* 20, 510–514.

Xu, H., Lan, J. H., Liu, B., Sheng, E. G., and Yeager, K. M. (2013). Modern carbon burial in lake qinghai, China. *Appl. Geochem.* 39, 150–155. doi: 10.1016/j.apgeochem.2013.04.004

Yu, Z. T., Wang, X. J., Zhao, C. Y., and Lan, H. Y. (2015). Carbon burial in Bosten Lake over the past century: impacts of climate change and human activity. *Chem. Geol.* 419, 132–141. doi: 10.1016/j.chemgeo.2015.10.037

Zhang, C. J., Sun, B. N., and Cui, Y. L. (2001). Thermolysis production of lake carbonatite organic matter and its carbon isotope composition characteristic. *J. Lanzhou Univer.* 37, 87–92.

Zhang, F. J., Xue, B., Yao, S. C., and Gui, Z. F. (2013). The organic carbon burial rates in Chinese lake sediments during Holocene Megathermal. *Quat. Sci.* 33, 401–402.

Zhang, F. J., Xue, B., Yao, S. C., and Gui, Z. F. (2018). Organic carbon burial from multi-core records in Hulun lake, the largest lake in northern China. *Quatern. Int.* 475, 80–90. doi: 10.1016/j.quaint.2017.12.005

Zhang, W. L., Yan, M. D., Fang, X. M., Zhang, D. W., Zhang, T., Zan, J. B., et al. (2019). High-resolution paleomagnetic constraint on the oldest hominoid- fossilbearing sequence in the Xiaolongtan Basin, southeast margin of the Tibetan Plateau and its geologic implications. *Global Planet. Change* 182:103001. doi: 10.1016/j.gloplacha.2019.103001

Zhang, Z. H., Zhao, M. X., Eglinton, G., Lu, H. Y., and Huang, C. Y. (2006). Leaf wax lipids as paleovegetational and paleoenvironmental proxies for the Chinese loess Plateauover the last 170 kyr. *Quat. Sci. Rev.* 25, 575–594. doi: 10.1016/j.quascirev.2005.03.009

Zheng, Y. H., Zhou, W. J., Meyers, P. A., and Xie, S. C. (2007). Lipid biomarkers in the Zoigê-Hongyuan peat deposit: indicators of holocene climate changes in West China. *Org. Geochem.* 38, 1927–1940. doi: 10.1016/j.orggeochem.2007.06.012

Zhong, N. N., Lu, S. F., Huang, Z. L., Zhang, Y. S., Xue, H. T., and Pan, C. C. (2004). Evolution of TOC of source rocks during the hydrocarbon generation process and its controlling factors. *Sci. China Earth Sci.* 34, 120–126.

Conflict of Interest: The authors declare that the research was conducted in the absence of any commercial or financial relationships that could be construed as a potential conflict of interest.